

Structural Properties of Chromium (Cr)-doped Titanium Dioxide (TiO₂) Nanoparticles prepared via Sol-gel Method at Different Temperatures

Nurul Huda Mohd Noor^{1,2}, Aishah Ain Nabila Mokhtar², Suraya Ahmad Kamil^{2,3}, Aida Fazliza Mat Fadzil^{1,2}, Mohamad Rusop Mahmood^{3,4} and Siti Nurbaya Supardan^{2,3*}

¹Centre of Foundation Studies, Universiti Teknologi MARA, Cawangan Selangor, Kampus Dengkil, 43800 Dengkil, Selangor, Malaysia

²Faculty of Applied Sciences, Universiti Teknologi MARA, 40450 Shah Alam, Selangor, Malaysia

³Centre for Functional Materials and Nanotechnology, Institute of Science (IoS), Universiti Teknologi MARA, 40450 Shah Alam, Selangor, Malaysia

⁴NANO-Electronic Centre, College of Engineering, Universiti Teknologi MARA, 40450 Shah Alam, Selangor, Malaysia

*Corresponding author (e-mail: sitinurbaya86@uitm.edu.my)

Titanium dioxide (TiO₂) as photocatalyst has gained much attention for environmental treatments due to its attractive characteristics. The applications of TiO₂ are significantly limited by its low visible light absorption, which is due to its large band gap. Doping TiO₂ with transition metal is one of the promising approaches to improve its photocatalytic efficiency by expanding its ultraviolet (UV) absorption to visible region. In this work, chromium (Cr)-doped TiO₂ nanoparticles (NPs) were prepared using sol-gel method at different calcination temperatures (400, 500, 600, and 700 °C). The structural properties for all samples were characterised using X-ray diffraction (XRD) and Fourier transform infrared (FTIR). XRD results show anatase phase observed in samples of pure TiO₂ and Cr-doped TiO₂ calcined at 400 °C. The rutile phase started to appear in sample of Cr-doped TiO₂ calcined at 500 °C to form mixed anatase-rutile phase. The minimum size of anatase was 17.38 nm at calcination temperatures of 400 and 500 °C, whereas rutile size was 22.22 nm at 500 °C. The largest specific surface area (SSA) of anatase was 88.04 m²·g⁻¹ at 400 °C and 500 °C, while for rutile was 64.43 m²·g⁻¹ at 500 °C. FTIR analysis shows the bonding changes that occurred with the introduction of Cr into TiO₂ nanoparticles.

Keywords: Titanium dioxide (TiO₂); chromium; Cr-doped TiO₂; sol-gel; anatase

Received: August 2022; Accepted: December 2022

Titanium dioxide (TiO₂) is a well-known and well-researched material due to the stability of its chemical structure, biocompatibility, and physical, optical, and electrical properties [1]. TiO₂ nanoparticles (NPs) have received great attention due to their outstanding performance in a wide range of applications [2]. In addition, among the semiconductors investigated for the purpose of pollutant degradation in water, TiO₂ is the most preferable material for the photocatalytic processes due to its high photosensitivity, nontoxic nature, large band gap, and stability [3]. TiO₂ properties are significantly dependent on the crystalline phase, i.e., anatase, rutile, or brookite [4]. TiO₂ has three polymorphs in anatase, rutile, and brookite, but anatase and rutile are the two main polymorphs that show various photocatalytic performances. Among these three crystalline phases of TiO₂, anatase is the most stable and more efficient in photocatalytic applications due to its open structure as compared with rutile phase [5]. Mixed-phase photocatalysts with rutile-anatase compositions have been reported to exhibit enhanced photoactivity relative to single-phase titania [6].

TiO₂ is widely used in photocatalytic applications because of its cost effectiveness and low impact method of removing organic impurities and non-biodegradable substances from wastewater. However, the wide band gap of TiO₂ makes it a less efficient photocatalytic material for the degradation of pollutants under visible light radiation and rapid recombination of photogenerated electron/hole pairs [7]. Furthermore, it is important to control the morphology and the crystal structure of TiO₂ since its photocatalytic activity is strongly dependent on the crystal structure, the crystallite size, and the specific surface area (SSA) [8][9].

Many approaches have been taken to modify TiO₂ such as metal coupling, dye sensitizer, and transition metal doping [10]. Transition metal doping such as chromium (Cr), vanadium (V), iron (Fe), zinc (Zn), nickel (Ni), and manganese (Mn) appears to be an effective method in enhancing the photocatalytic activity of TiO₂ due to their ability to enhance the photocatalytic activity by delaying the combination of photogenerated electrons and holes or enhancing the

adsorption activity [11]. Cr is one of the most commonly used dopants in TiO₂ as it has been shown to improve photocurrent density with a shift in optical absorption in the visible range because Cr³⁺ ions have fewer valence electrons than Ti⁴⁺, and the excess of holes creates an acceptor level near the TiO₂ valence band [12]. Moreover, the doping of Cr³⁺ ions can decrease the crystal size of TiO₂ and shift the valence band maximum upwards and lead to strong visible-light absorption and thus will decrease the recombination rate [13]. Furthermore, Cr/TiO₂ nanotubes have shown obvious absorption in visible region and have higher photocatalytic activities for degradation of methyl orange under the ultraviolet-visible light irradiation [14].

Various techniques such as the sol-gel method, chemical vapor decomposition method, hydrothermal technique, and reversed micelle method have been used to synthesise TiO₂ NPs [15]. The sol-gel process has been widely used in the preparation of the surface and interface-controlled materials made from ceramics, glass materials, and fibres. Moreover, the sol-gel method has been extensively used in the preparation of doped TiO₂ photocatalysts, resulting in high crystallinity and surface area [9]. These advantages make sol-gel one of the best techniques used for TiO₂ synthesis. However, the preparation parameters such as solvent, water content, precursor type, pH solution, viscosity, aging conditions, drying, and calcination temperature affect the properties of the powder synthesised using sol-gel [16]. Therefore, the present study reports a simple synthesis method for the preparation of TiO₂ NPs and investigates the effect of different calcination temperatures on the structural properties of Cr-doped TiO₂ NPs prepared by the sol-gel method. The effects of Cr-doping on the crystallite size, structure, and phase composition of the synthesised samples were investigated by XRD. FTIR spectroscopy was used to collect information about the molecular geometry, functional groups, and inter- or intra-molecular interactions in the sample.

EXPERIMENTAL

1. Chemicals and Materials

The following reagents were used as received without additional purification: titanium (IV) butoxide (TTIB) (Aldrich, 97%), ethanol (C₂H₅OH), chromium (III) nitrate nonahydrate (Cr(NO₃)₃·9H₂O) (Aldrich, 99%), 1 M nitric acid (HNO₃), and deionised water.

2. Characterisation Method

TiO₂ NPs were synthesised via sol-gel technique at room temperature (25 °C), and the preparation method was adopted from N. R. Mathews et al. [17] with some modifications. A mixture of 5 mL deionised water and 55 mL ethanol was added drop by drop into the solution containing 26 mL of titanium (IV) butoxide

and 55 mL ethanol and stirred for 1 h. The solution was continuously stirred for another 4 h at room temperature (25 °C) at 200–400 rpm. Acidity of the solution was controlled by adding HNO₃ dropwise to attain pH of 2.0. Then, the solution was stirred for another 1 h. For the solution with Cr doping, the appropriate amount of Cr(NO₃)₃ was added into the precursor solution to give a concentration of 1.0 wt.% of Cr-doped TiO₂, and it was then peptized overnight to get 2 layers of the solution. Then the solution was filtered, leaving behind an amount of titanic gel. The titanic gel was dried on a hot plate at 120 °C for 1.5 h until the powder was formed. The powder was then pulverised using ball milling at 900 rpm for 3 h to obtain TiO₂ NPs. The powder samples were calcined at 400, 500, 600, and 700 °C (heating rate of 5 °C/min) for 3 h.

RESULTS AND DISCUSSION

XRD technique (PANalytical X'Pert Pro) using Cu K α radiation was employed to determine the phase and crystal structure of TiO₂ NPs. The diffractometer data were recorded by scanning 2 θ from 10 °C. The crystallite size was obtained by using the Debye-Scherrer equation from the XRD analysis [18][19]. This equation is a well-known method for calculating the crystallite size based on the line broadening for the XRD peaks at their full width at half maximum (FWHM). The average crystallite size (D) for TiO₂ NPs was calculated by the Debye-Scherrer formula given in Equation (1):

$$D = \frac{0.9 \lambda}{\beta \cos \theta} \quad (1)$$

where D = average crystallite size, λ = X-ray wavelength, 0.9 is the Scherrer constant, β =FWHM, and θ = corresponding diffraction angle. Thus, using that equation, the phase and crystallinity of TiO₂ can be examined.

FTIR was used to determine the molecular structure and chemical bonding in the prepared samples [20]. FTIR can be divided into two regions which is functional group region and fingerprint region. The specific functional group can be determined in the wavenumber range at 4000 to 1500 cm⁻¹, while the fingerprint region can be examined from 1500 to 500 cm⁻¹. The transmission of the sample was measured because it represents the light absorbed by the molecule. The energy from the light causes the bond to vibrate, and the bond vibration can be divided into several types such as bond stretching, bending, rocking, and twisting. The functional group have their respective wavenumber [21]. Therefore, the peak present at the wavenumber in the functional group region can be determined by comparing with the standard wavenumber of the functional group. FTIR spectrometer (Perkin Elmer Spectrum 400 FTIR/FT-NIR) was used to

measure the transmission of the sample with the scan range of 4000–450 cm⁻¹.

1. X-Ray Diffraction (XRD)

The XRD patterns for pure TiO₂ NPs and Cr-doped TiO₂ with 1 wt.% of Cr ions calcined at different temperatures of 400, 500, 600, and 700 °C were compared to the reference from ICSD using POWD-12++ (1997). Figure 1 shows the XRD pattern of pure TiO₂ NPs calcined at 500 °C and Cr-doped TiO₂ calcined at different temperatures from 400 to 700 °C. The anatase phase is stable at low temperatures (400–500 °C) without the addition of chromium (undoped TiO₂), therefore pure TiO₂ was calcined at 500 °C because the transition of anatase–rutile depends on the heating temperature [22][23]. The anatase structure appeared for all samples whose crystal planes were (101), (200), (211), (204), (220), and (215). First, all patterns for Cr-doped TiO₂ calcined at 400 °C sample exclusively show diffraction peaks that correspond to anatase structure (ICSD using POWD-12++, space group I41/amd). The structural phase transition was observed when rutile started to coexist with anatase as the calcination temperature increased. At temperatures from 500 to 700 °C, the diffraction pattern showed a mixture of crystalline phases of anatase and rutile. As the temperature was increased to 500 °C, rutile started

to appear which was at (210), (211), and (301). The dominant peak of rutile at 500 °C was 25.367° (211), and the dominant peaks of rutile at 600 and 700 °C were 27.440° (110) and 27.508° (110), respectively (ICSD using POWD-12++, space group, P42/mnm). Our results are similar to a previous work that reported all of the patterns of the samples calcined at 400 °C show an anatase structure [6][24]. When the temperature was increased to 800 °C, the anatase structure changed to rutile structure. Cr-doping resulted in the complete disappearance of the anatase phases due to higher calcination temperature [25]. Therefore, doping Cr into TiO₂ has a significant effect on the structural property of TiO₂ and changes its structural phase from anatase to mixed anatase–rutile. The calcination temperature is also a parameter that influences structural property. In sol-gel synthesis, heat treatment plays a vital role because it alters the phase composition in terms of both microstructural and morphological properties of the nanocomposites at different stages [26]. These properties can be varied based on the synthesis temperature, post-synthesis (annealing) treatments, or time durations of such heat treatments [27]. Intensity is proportional to temperature; as a result, as the annealing temperature is increased, the rutile phase appears. The highest intensity was observed at 600 °C compared to samples for other different calcination temperatures [19].

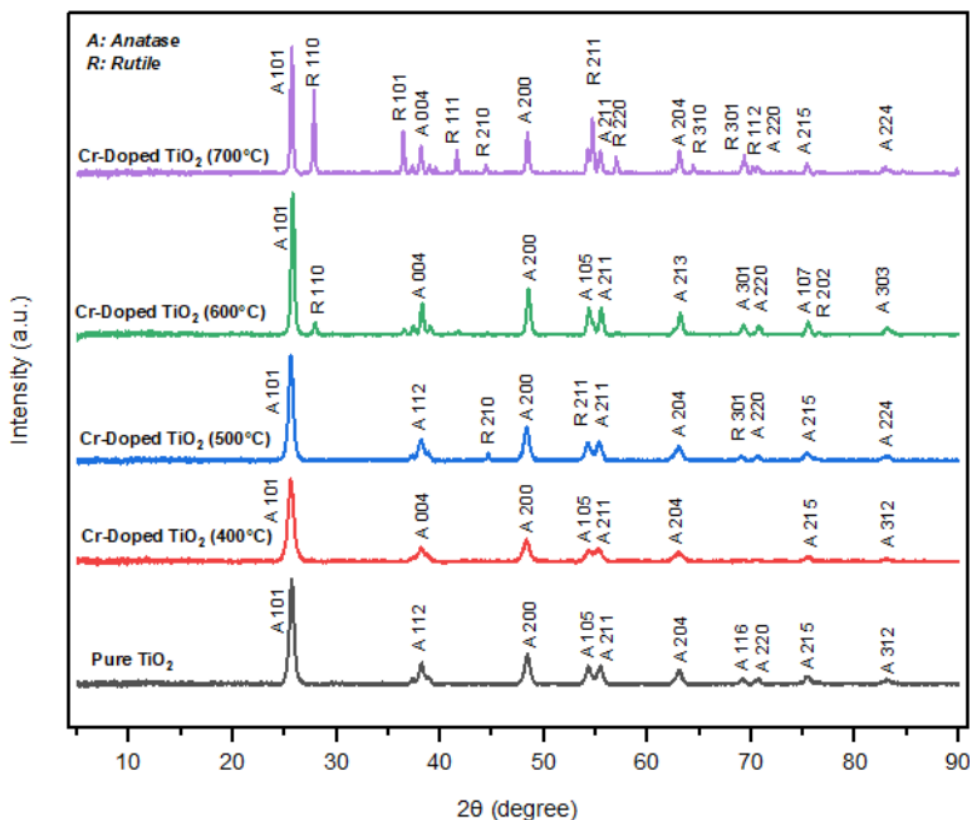


Figure 1. The XRD pattern of pure TiO₂ (calcined at 500 °C) and Cr-doped TiO₂ calcined at different temperatures.

The mole ratios of the anatase and rutile phases were calculated based on the Spurr and Myers equations (2) and (3) [19] using the most intense peak of each phase. Next, the SSA was calculated as the total area covered by the crystals in unit mass as shown in equation (6). The density is denoted by ρ , while D_p denotes the size of the crystals obtained from the Debye-Scherrer equation.

$$W_R = \frac{1}{1+0.8\left(\frac{I_A}{I_R}\right)} \quad (2)$$

$$W_A = 1 - W_R \quad (3)$$

$$\text{Anatase \%} = \frac{100 \times I_A}{I_A + 1.265 \times I_R} \quad (4)$$

$$100 - A\% = \text{Rutile \%} \quad (5)$$

$$SSA = \frac{6 \times 10^3}{\rho D_p} \quad (6)$$

$$\rho = \frac{1}{D_p^2} \quad (7)$$

W_R and I_R represent the mole fraction and intensity of the rutile phase, respectively, while W_A and I_A are the mole fraction and intensity of the anatase phase, respectively. The phase contents of anatase (101) and rutile (110) were obtained using equations (4) and (5). I_A and I_R represent the intensity of the anatase (101) and rutile (110) phases, respectively. Tables 1, 2 and 3 represent full width at half maximum (FWHM) and crystallite size of anatase peak and rutile peak, phase content.

Table 1. FWHM and crystallite size of anatase and rutile peak.

Temperature (°C)	Anatase		Rutile	
	FWHM (degree)	Crystallite size (nm)	FWHM (degree)	Crystallite size (nm)
400	0.4684	17.38	0	0
500	0.4684	17.38	0.4015	22.22
600	0.1224	66.55	0.2856	28.65
700	0.2175	37.45	0.1840	44.46

Table 2. Phase content of anatase and rutile.

Temperature (°C)	Ratio Anatase	Ratio Rutile
Pure TiO ₂	100	0
400	100	0
500	82	18
600	90	10
700	55	45

Table 3. Crystallite size and SSA of anatase and rutile peak.

Temperature (°C)	Anatase		Rutile	
	Crystalline Size (nm)	SSA (m ² g ⁻¹)	Crystalline Size (nm)	SSA (m ² g ⁻¹)
400	17.38	88.04	0	0
500	17.38	88.04	22.22	64.44
600	66.55	22.15	28.65	49.27
700	37.45	40.87	44.46	31.53

The obtained XRD pattern in Fig. 1 was used to calculate the weight fraction of anatase and rutile using Spurr equation. The percentage ratios for pure TiO₂ and Cr-doped TiO₂ calcined at 400, 500, 600, and 700 °C were 1:0, 1:0, 8:2, 9:1, and 6:4, respectively. Figure 2 shows the phase content of pure TiO₂ and Cr-doped TiO₂ NPs calcined at different temperatures. Both phases are reciprocal. Therefore, it was concluded that anatase content decreases with an increase in annealing temperature while rutile content increases [21].

The crystallite size of the calcined powders varied depending on the calcination temperature, which ranged from 400 to 700 °C. From the XRD result, the crystallite size of anatase at 400 and 500 °C were stable because the sizes remain unchanged. The maximum anatase size was 66.55 nm from the sample calcined at

600 °C. When the temperature was higher than 600 °C, the size of anatase decreased while rutile size increased. The crystallite size of rutile increased significantly as the temperature increased, and the maximum rutile size was 44.46 nm for the calcination temperature of 700 °C as shown in Fig. 3. Smaller crystallite sizes lead to better photocatalytic performance due to an enhanced e⁻/h⁺ recombination rate via decreasing the distance for charge carriers to reach the surface without recombination [16]. Moreover, for small sized photocatalysts, the path of the charge to migrate to photocatalyst surface decreases, resulting in a decrease of the recombination rate of the charge carriers. Since oxidation/reduction reactions have to take place at the surface, increasing the specific surface area increases the number of possible reaction sites and decreases the distance separated charges must travel to reach the nearest surface [28].

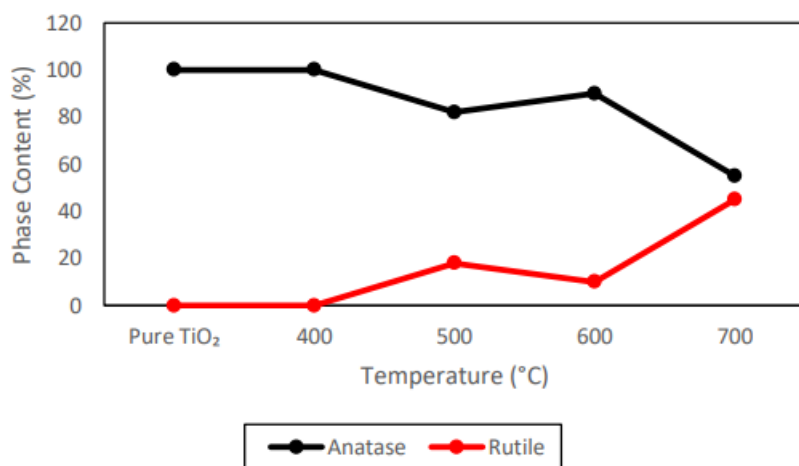


Figure 2. Phase content of pure TiO₂ and Cr-doped TiO₂ NPs calcined at different temperatures.

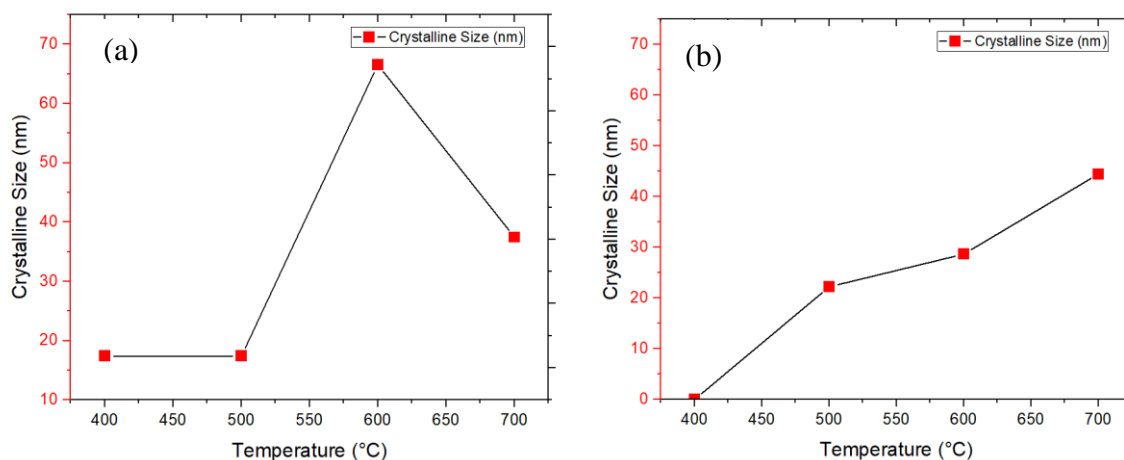


Figure 3. Crystallite size of Cr-doped TiO₂ NPs calcined at different temperatures for (a) anatase, (b) rutile.

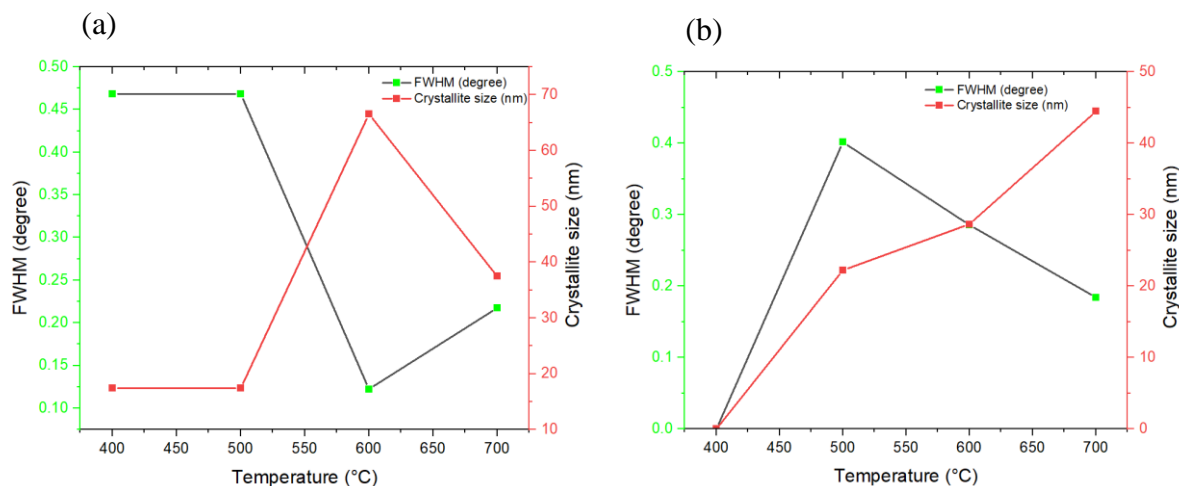
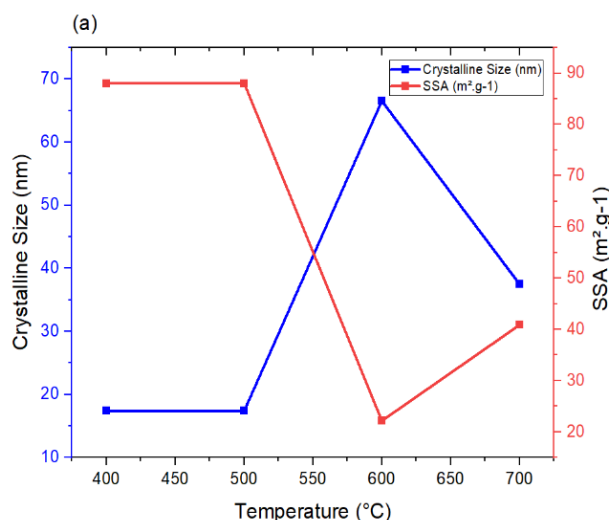


Figure 4. The FWHM and crystallite size of Cr-doped TiO₂ NPs annealed at different temperatures for (a) anatase, (b) rutile.

The crystallite sizes for all samples were calculated based on the FWHM value from XRD data using Scherrer equation. The size is inversely proportional to FWHM. When the size increases, the FWHM decreases as shown in Fig. 4. Furthermore, the densities (Eq. 6) of anatase and rutile for pure TiO₂ were 3.92 and 4.23 g/cm³, respectively. At 400 °C, densities of anatase and rutile were 3.92 and 4.25 g/cm³, respectively, whereas at 500 °C, anatase had a density of 3.92 g/cm³ and rutile had a density of 4.19 g/cm³. Next, at 600 °C, the densities of anatase and rutile were 4.07 and 4.25 g/cm³, respectively, while at 700 °C, the densities of anatase and rutile were 4.28 and 3.92 g/cm³, respectively. Next, SSA (Eq. 5) was calculated as

the total area covered by the crystals in unit mass. In the anatase phase, the SSA value of Cr-doped TiO₂ NPs decreased from 88.04263 to 40.87017 m²·g⁻¹ after calcination at temperatures ranging from 400 to 700 °C. SSA values for rutile phase at 500, 600, and 700 °C were 64.43863, 49.27333, and 31.52896 m²·g⁻¹, respectively. At 500 °C, the rutile phase was observed stable. SSA was calculated by considering the total area covered by the crystals in unit mass. As the calcination temperature increases, SSA decreases, thus lowering photocatalytic activity. In reverse, when SSA increases, the photocatalytic activity increases [18]. Figure 5 shows the crystallite size and SSA of Cr-doped TiO₂ NPs calcined at different temperatures for anatase and rutile phases.



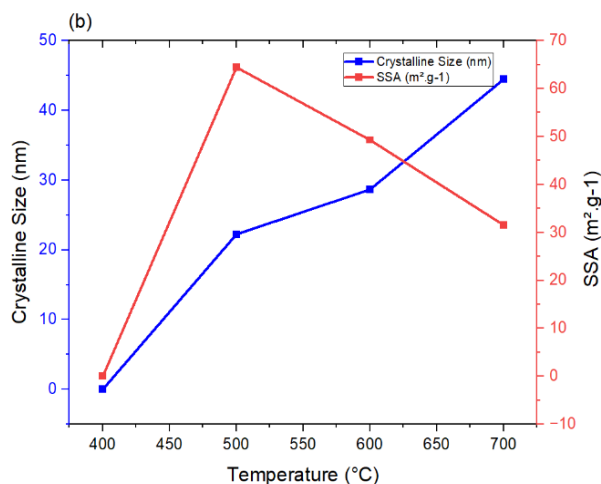


Figure 5: The crystallite size and SSA of Cr-doped TiO₂ NPs annealed at different temperatures for (a) anatase, (b) rutile.

2. Fourier Transform Infrared (FTIR)

To identify the vibrational bands, the peaks in the region of 500–4000 cm⁻¹ were recorded and displayed in Fig. 6. Figure 6 shows the absorption spectra of undoped TiO₂ and Cr-doped TiO₂ NPs calcined at 400, 500, 600, and 700°C. The peaks in the region of 4000–500 cm⁻¹ are characteristic of IR-active fundamental and combination lattice modes of crystalline Cr and Ti oxides [21]. The peak intensity and band position of the spectra depend on the crystal structure, chemical composition, and morphology of the sample [29]. The peak positions in an infrared spectrum are used to distinguish different functional groups from each other. Different functional groups can have peaks at about the same position. Generally, metal-oxide (M-O) shows peaks in fingerprint region [9]. The FTIR spectrum for the OH stretching region is observed in the range 3352–3820 cm⁻¹ [20][30] which corresponds to the

bending and stretching modes of the –OH groups of absorbed molecular water, indicating that the sample is hydrolysed [31]. In the spectra, a very sharp absorption peak at 698 cm⁻¹ for Cr-doped TiO₂ NPs calcined at 500 °C is due to the Ti–O–Ti bond of anatase titanium [32]. Wide band in the range of 450–700 cm⁻¹ combines stretching modes of Ti–O–Ti bonds which are typical for titanium oxides (Kumar et al., 2000). The band around 548–698 cm⁻¹ is attributed to Ti–O stretching vibration. The 698.0 cm⁻¹ peak shifted to the higher wavelength by adding transition metal [33]. As the calcination temperature increased, this peak shifted to a lower frequency region, indicating the disruption of the Ti–O–O bond and the creation of Ti–O bond [1]. The peak around 1000 cm⁻¹ for the samples calcined at 600 and 700 °C can be also attributed to the lattice vibrations of rutile [30]. This is in agreement with the XRD data analysis discussed previously.

Table 4. Chemical bonding of each wavenumber.

Wavenumbers (cm ⁻¹)	Bonding	References
3820.0	OH	[20][31]
3453.5	OH	[30]
698.0	Ti-O-Ti	[32]
622.1	Ti-O-Ti	[33]
680.6	Ti-O	[1]

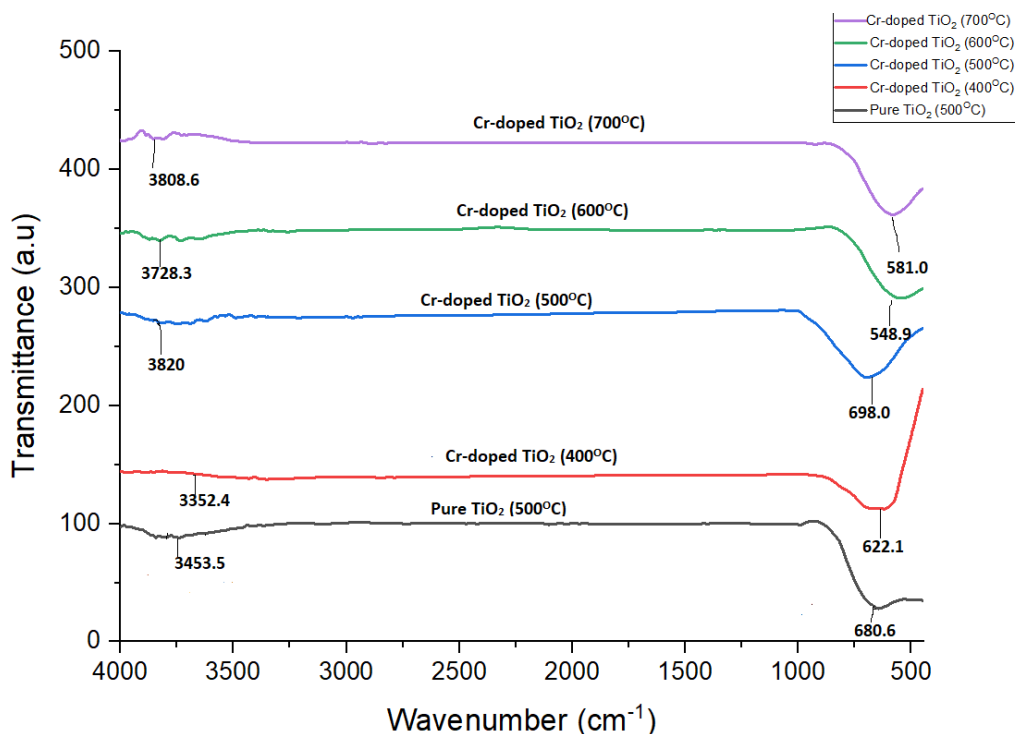


Figure 6. FTIR spectra of pure TiO₂ and Cr-doped TiO₂ NPs obtained from various calcination temperatures.

CONCLUSION

The calcination temperature was found to have a transformative effect on the structural properties of Cr-doped TiO₂ nanoparticles. The metastable anatase phase transformed to mixed anatase–rutile phase at around 500 °C. XRD results found that the particle sizes increased with an increase in calcination temperature. Therefore, calcination temperature improves the nanoparticles crystallinity, causes phase transformation, and affects photocatalytic activity. FTIR study shows the bands related Ti–O–Ti vibrations shifted to higher wavelength with Cr doping. Moreover, a significant peak was observed related to the stretching vibration mode of the -OH group of surface-absorbed water. Our study suggests that 500 °C is the optimum calcination temperature for the synthesis of Cr-doped TiO₂ NP via sol-gel method.

ACKNOWLEDGEMENTS

Authors would like to thank Universiti Teknologi MARA for the financial support through the grant (No. 600-RMC/GPK 5/3 (190/2020)). The authors also acknowledge the Faculty of Applied Sciences for the experimental and characterisation facilities.

REFERENCES

1. Anitha, B. and Khadar, M. A. (2020) Anatase-rutile phase transformation and photocatalysis in peroxide gel route prepared TiO₂ nanocrystals: Role of defect states. *Solid State Sci.*, **108**, 106392, February, 2020. doi: 10.1016/j.solidstatesciences.

2020.106392.

2. Abbas, F. and Bensaha, R. (2020) Effect of annealing time on structural and optical properties of mercury (Hg+2) doped TiO₂ thin films elaborated by sol-gel method for future photocatalytic application. *Optik (Stuttg)*, **247**, 167846, August 2021. doi: 10.1016/j.ijleo.2021.167846.
3. Prekajski, M., *et al.* (2016) Synthesis and characterization of Cr³⁺ doped TiO₂ nanometric powders. *Ceram. Int.*, **42**, 1, 1862–1869. doi: 10.1016/j.ceramint.2015.09.151.
4. Asiah, M. N., Basri, M. Z. and Rusop, M. (2011) Electrical properties of nanostructured titanium dioxide thin films prepared by sol-gel spin-coating method. *Defect Diffus. Forum*, 312–315, 1027–1031. doi: 10.4028/www.scientific.net/DDF.312-315.1027.
5. Us Saqib, N., Adnan, R. and Shah, I. (2016) A mini-review on rare earth metal-doped TiO₂ for photocatalytic remediation of wastewater. *Environ. Sci. Pollut. Res.*, **23**, 16, 15941–15951, August 2016. doi: 10.1007/s11356-016-6984-7.
6. Hanaor, D. A. H. and Sorrell, C. C. (2011) Review of the anatase to rutile phase transformation. *J. Mater. Sci.*, **46**, 4, 855–874. doi: 10.1007/s10853-010-5113-0.
7. Manzoor, M., Rafiq, A., Ikram, M., Nafees, M. and Ali, S. (2018) Structural, optical, and magnetic

- study of Ni-doped TiO₂ nanoparticles synthesized by sol-gel method. *Int. Nano Lett.*, **8**, 1, 1–8. doi: 10.1007/s40089-018-0225-7.
8. Hao, B., Guo, J., Zhang, L. and Ma, H. (2021) Cr-doped TiO₂/CuO photocatalytic nanofilms prepared by magnetron sputtering for wastewater treatment. *Ceram. Int.*, November, 2021. doi: 10.1016/J.CERAMINT.2021.11.270.
 9. Guo, W. L., Wang, X. K., Lin, Z. M. and Song, G. Z. (2002) Sonochemical Synthesis of Nanocrystalline TiO₂ by Hydrolysis of Titanium Alkoxides. *Kao Teng Hsueh Hsiao Hua Heush Hsueh Pao/ Chem. J. Chinese Univ.*, **23**, 8, 1593–1594,
 10. Koh, P. W., Yuliaty, L. and Lee, S. L. (2014) Effect of transition metal oxide doping (Cr, Co, V) in the photocatalytic activity of TiO₂ for congo red degradation under visible light. *J. Teknol. (Sciences Eng.)*, **69**, 5, 45–50. doi: 10.11113/jt.v69.3203.
 11. Zhou, X., Lu, J., Li, L. and Wang, Z. (2011) Preparation of crystalline Sn-Doped TiO₂ and its application in visible-light photocatalysis. *J. Nanomater.*, 2011. doi: 10.1155/2011/432947.
 12. Hajjaji, A., *et al.* (2014) Cr-Doped TiO₂ Thin Films Prepared by Means of a Magnetron Co-Sputtering Process: Photocatalytic Application. *Am. J. Anal. Chem.*, **5**, 8, 473–482. doi: 10.4236/ajac.2014.58056.
 13. Li, X., Guo, Z. and He, T. (2013) The doping mechanism of Cr into TiO₂ and its influence on the photocatalytic performance. *Phys. Chem. Chem. Phys.*, **15**, 46, 20037–20045, Dec. 2013. doi: 10.1039/c3cp53531b.
 14. Zhang, S., *et al.* Synthesis, characterization of Cr-doped TiO₂ nanotubes with high photocatalytic activity. doi: 10.1007/s11051-007-9309-4.
 15. Hasan, F. (2019) Synthesis of Cr Doped TiO₂ Using Sol-Gel Technique and Calculation of its Photocatalytic Activity * Address for Correspondence Synthesis of Cr Doped TiO₂ Using Sol-Gel Technique and Calculation of its Photocatalytic Activity. June, 2019.
 16. Agartan, L., Kapsuz, D., Park, J. and Ozturk, A. (2015) Effect of initial water content and calcination temperature on photocatalytic properties of TiO₂ nanopowders synthesized by the sol-gel process. *Ceram. Int.*, **41**, 10, 12788–12797. doi: 10.1016/j.ceramint.2015.06.114.
 17. Mathews, N. R., Morales, E. R., Cortés-Jacome, M. A. and Toledo Antonio, J. A. (2009) TiO₂ thin films - Influence of annealing temperature on structural, optical and photocatalytic properties. *Sol. Energy*, **83**, 9, 1499–1508. doi: 10.1016/j.solener.2009.04.008.
 18. Muthee, D. K. and Dejene, B. F. (2021) Effect of annealing temperature on structural, optical, and photocatalytic properties of titanium dioxide nanoparticles. *Heliyon*, **7**, 6, e07269. doi: 10.1016/j.heliyon.2021.e07269.
 19. Khalid Hossain, M., *et al.* (2017) Annealing temperature effect on structural, morphological and optical parameters of mesoporous TiO₂ film photoanode for dye-sensitized solar cell application. *Mater. Sci. Pol.*, **35**, 4, 868–877. doi: 10.1515/msp-2017-0082.
 20. Kumar, M. M., Badrinarayanan, S. and Sastry, M. (2000) Nanocrystalline TiO₂ studied by optical, FTIR and X-ray photoelectron spectroscopy: Correlation to presence of surface states. *Thin Solid Films*, **358**, 1, 122–130. doi: 10.1016/S0040-6090(99)00722-1.
 21. Khaleel, A., Shehadi, I. and Al-Shamisi, M. (2010) Structural and textural characterization of sol-gel prepared nanoscale titanium-chromium mixed oxides. *J. Non. Cryst. Solids*, **356**, 25–27, 1282–1287. doi: 10.1016/j.jnoncrystol.2010.04.031.
 22. Bellifa, A., Choukchou-Braham, A., Kappenstein, C. and Pirault-Roy, L. (2014) Study of the effect of transition metals on titanium dioxide phase transformation. *Springer Proc. Phys.*, **155**, 3, 1–7. doi: 10.1007/978-3-319-05521-3_1.
 23. Dubey, R. S. and Singh, S. (2017) Investigation of structural and optical properties of pure and chromium doped TiO₂ nanoparticles prepared by solvothermal method. *Results Phys.*, **7**, March, 1283–1288. doi: 10.1016/j.rinp.2017.03.014.
 24. Kim, M. G., *et al.* (2021) Effects of Calcination Temperature on the Phase Composition, Photocatalytic Degradation, and Virucidal Activities of TiO₂ Nanoparticles. *ACS Omega*, **6**, 16, 10668–10678. doi: 10.1021/acsomega.1c00043.
 25. Naseem, S. *et al.* (2019) Enhanced Photocatalytic Activity by Tuning of Structural and Optoelectrical Properties of Cr(III) Incorporated TiO₂ Nanoparticles. *J. Electron. Mater.*, **48**, 11, 7203–7215. doi: 10.1007/s11664-019-07499-7.
 26. Yan, X., Zhao, C. L., Zhou, Y. L., Wu, Z. J., Yuan, J. M. and Li, W. S. (2015) Synthesis and characterization of ZnTiO₃ with high photocatalytic activity. *Trans. Nonferrous Met. Soc. China (English Ed.)*, **25**, 7, 2272–2278. doi: 10.1016/S1003-6326(15)63841-9.
 27. Munguti, L. and Dejene, F. (2020) Influence of annealing temperature on structural, optical and

- photocatalytic properties of ZnO–TiO₂ composites for application in dye removal in water. *Nano-Structures and Nano-Objects*, **24**, 100594. doi: 10.1016/j.nanoso.2020.100594.
28. Ramaswamy, V., Jagtap, N. B., Vijayanand, S., Bhange, D. S. and Awati, P. S. (2008) Photocatalytic decomposition of methylene blue on nanocrystalline titania prepared by different methods. *Mater. Res. Bull.*, **43**, 5, 1145–1152. doi: 10.1016/j.materresbull.2007.06.003.
29. Irshad, K., Tahir, Khan, M. and Murtaza, A. (2018) Synthesis and characterization of transition-metals-doped ZnO nanoparticles by sol-gel auto-combustion method. doi: 10.1016/j.physb.2018.05.006.
30. Kotsyubynsky, V., Myronyuk, I., Chelyadyn, V., Hrubciak, A., Moklyak, V. and Fedorchenko, S. (2017) Rod-like rutile nanoparticles: Synthesis, structure and morphology. *J. Nano Res.*, **50**, 32–40. doi: 10.4028/www.scientific.net/JNanoR.50.32.
31. Demirci, S., Dikici, T., Yurddaskal, M., Gultekin, S., Toparli, M. and Celik, E. (2016) Synthesis and characterization of Ag doped TiO₂ heterojunction films and their photocatalytic performances. *Appl. Surf. Sci.*, **390**, 591–601. doi: 10.1016/j.apsusc.2016.08.145.
32. Goswami, P. and Ganguli, J. N. (2013) Tuning the band gap of mesoporous Zr-doped TiO₂ for effective degradation of pesticide quinalphos. **42**, 40.
33. Ghasemi, S., Rahimnejad, S., Setayesh, S. R., Rohani, S. and Gholami, M. R. (2009) Transition metal ions effect on the properties and photocatalytic activity of nanocrystalline TiO₂ prepared in an ionic liquid. *J. Hazard. Mater.*, **172**, 2–3, 1573–1578. doi: 10.1016/j.jhazmat.2009.08.029.